

Stochastic dynamics of granular hopper flows: a slow hidden mode controls the stability of clogs

David Hathcock,¹ Sam Dillavou,² Jesse M. Hanlan,² Douglas J. Durian,² and Yuhai Tu¹

¹*IBM T. J. Watson Research Center, Yorktown Heights, NY 10598, USA*

²*Department of Physics & Astronomy, University of Pennsylvania, Philadelphia, PA 19104, USA*

(Dated: October 5, 2024)

Granular flows in small-outlet hoppers exhibit intermittent clogging behavior: while a temporary clog (pause) can last for an extended period before flow spontaneously restarts, there are also permanent clogs that last beyond experimental timescales. Here, we introduce a phenomenological model with multiplicative noise that provides a dynamical explanation for these extreme events: they arise due to coupling between the flow rate and a slow hidden mode that controls the stability of clogs. The theory fully resolves the statistics of pause and clog events, including the non-exponential clogging times and non-Gaussian flow rate distribution and explains the stretched-exponential growth of the average clogging time with outlet size. Our work provides a framework for extracting features of granular flow dynamics from experimental trajectories.

Clogging in granular hopper flows is an extreme event, where the formation of a stable arch by a small number of grains near the outlet entirely stops the motion of the bulk material [1–4]. Similar phenomena appear across scales in systems moving through narrow bottlenecks, from suspensions [5–9] and collections of cells [9–11] to human and animal crowds [4, 12, 13]. The dependence of flows and clogging on grain properties [3, 14–19] and hopper geometry [3, 18–24] have been extensively studied. Nonetheless, many statistical properties of granular flows remain unexplained and clogs cannot be reliably predicted.

The dynamics and duration of granular flows depends strongly on the hopper outlet size [21]. For small outlets, where clogs form quickly, flows have a few characteristic features. First, the magnitude of fluctuations in the flow rate grow (relative to the mean) and become markedly non-Gaussian [25–27]. Second, temporary clogs (pauses) emerge, during which a metastable arch forms and flow is suspended for an extended period, before continuous flow spontaneously restarts. This behavior has primarily been studied in granular systems perturbed by external vibrations [4, 23, 28–31] or coupling to fluid dynamics [8, 32], but fully spontaneous unclogging is also possible [25, 26, 33]. Understanding the flow statistics and relation between clogs and pauses will provide insight into the dynamics preceding a clog.

In this Letter, we introduce a minimal phenomenological model for the stochastic dynamics of granular flows. The flow rate fluctuates according to Langevin dynamics with multiplicative noise and has an absorbing state representing a clog. The model predicts the statistics of the flow-rate, clogging time, mass ejected, and number of pauses, all of which are confirmed by our large collection of measured flows ($\sim 50,000$ over 5 outlet sizes).

One of our key findings is that coupling to a hidden mode—perhaps a slow configurational degree of freedom—explains the emergence of intermittent pauses in the flow and the resulting non-Gaussian flow-rate dis-

tribution and non-exponential clogging times. This hidden mode controls the stability of clogs. As the flow rate approaches zero, it performs independent Bernoulli trials, whose outcome is determined by the state of the hidden variable, to determine whether the system clogs or pauses. Our results indicate that a single order-parameter, corresponding to our hidden variable, enables advanced prediction of whether a zero-flow-rate event will be a temporary or permanent clog.

The experimental data in this study were collected using an automated recirculating hopper. The apparatus, data set, and procedures are described in detail in [34]. Briefly, the hopper shown in Fig. 1(a) is a vertical quasi-2D plexiglass cell containing an ensemble of tri-disperse anti-static polyethylene disks with diameters, $d_S = 6.0$ mm, $d_M = 7.4$ mm, $d_L = 8.6$ mm, and equal heights. The disks form a single layer, and flow through an opening until they spontaneously clog. Grain positions are recorded by a camera at 130 fps and tracked using custom MATLAB software. Mass ejected over time $M(t)$ is calculated as the total mass of particles that passes a semi-circular boundary spanning and centered on the outlet. This permits ignorance of particles in the center of the outlet, which are the most difficult to track. Flow rate $W(t)$ is then calculated at each frame by taking the slope of a second-order polynomial fit to small sections of data (approximately five frames). The choice of fit window and weighting scheme (Gaussian around central point with standard deviation of one frame) have minimal effect on the outcome of $W(t)$.

Flows are initiated via mechanical vibration using a speaker near the outlet. The flow is recorded and tracked, and is considered complete when no grains fall through the outlet for five seconds. Ejected grains are directed into a chute to one side, and recirculated into the top of the hopper by a continuous air stream directed upwards. This chute is placed sufficiently far away from the outlet such that it does not disturb the flow there. The connection from the recirculation motor is a constant

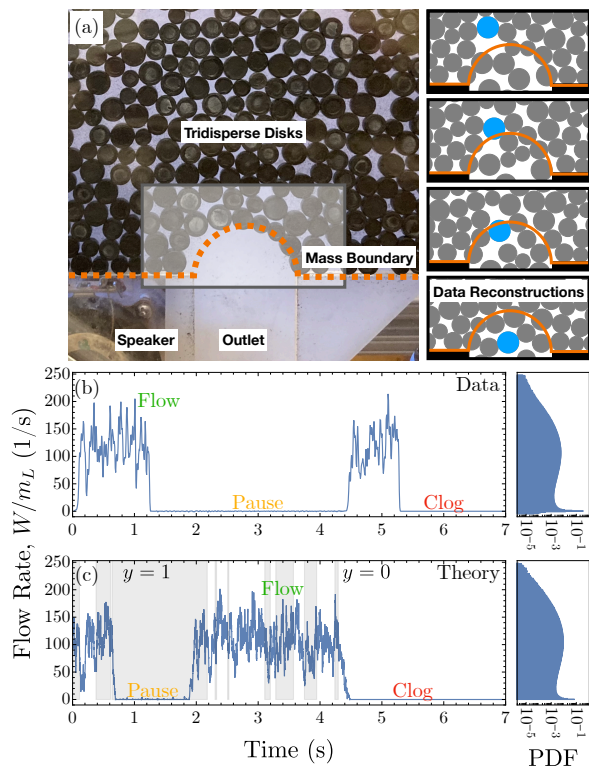


FIG. 1. (a) Image of the experimental system along and snapshots of reconstructed data. The mass boundary line is shown in orange. A large particle is highlighted in blue in the reconstruction, which shows four snapshots separated by 3 frames ($\Delta t = 3/130 \approx 23\text{ms}$). When a grain straddles the mass boundary line, only a fraction of its mass is counted as ejected. (b) An experimental flow-rate trajectory, $W(t)$, with a single pause. The histogram shows the distribution of flow rates across all $D = 3.86d_L$ flows. (c) A trajectory and flow-rate distribution from simulations of the Langevin model, Eqs. (1) & (2). The background color indicates the hidden variable state, $y = 0$ (white) and $y = 1$ (gray).

source of small vibrations in the hopper, which increases the frequency of temporary pauses; 38% of flows have at least one pause. This low-level vibration is far smaller than the vibration used to restart the flow. Using this automation scheme, the experiment can continuously run without human intervention. Over 50,000 flows with outlet width $D = 3.86d_L$ were autonomously recorded over months, along with at least one thousand experiments each for four additional outlet sizes. About 21% of flows pause once before clogging permanently; Fig. 1(b) shows a typical trajectory in this category.

Systems with absorbing states (e.g., autocatalytic chemical processes) have been successfully modeled by Langevin equations with multiplicative noise [35, 36]. To capture the hopper flow statistics, we adopt this approach: the flow rate fluctuates according to Langevin dynamics with multiplicative noise. However, in order to distinguish the pause and clog states, we introduce a hid-

den variable coupled to the flow rate. The instantaneous flow rate in the hopper, $x = W/m_L$, evolves according to,

$$\dot{x} = f(x) + \sqrt{2(g(x) + \epsilon y)} \eta(t). \quad (1)$$

Here, $f(x)$ is the deterministic force, $g(x)$ is the noise amplitude (which depends on the flow rate), y is a hidden variable, and $\eta(t)$ is the Gaussian white noise with mean and correlation $\langle \eta(t) \rangle = 0$ and $\langle \eta(t)\eta(t') \rangle = \delta(t - t')$ respectively. We require $f(0)=g(0)=0$, so that $x = 0$ is an absorbing state when $y = 0$. Expanding to linear order, we have $g(x) = \Delta x/x_0$. We use force, $f(x) = -x^2(x - x_0)\Psi(x)/(\tau_0 x_0^2)$, which has zeros at the clog $x = 0$ and steady flow rate x_0 [37]. Here τ_0 is the correlation time at $x = x_0$ and $\Psi(x)$ is a positive-definite function that allows deformations of the force [38].

For simplicity, we assume the hidden variable y is a binary variable with states $y = 0, 1$ and switching rates $r_0(x)$ and $r_1(x)$ that depend on the flow rate x ,

$$y : \quad 0 \xrightleftharpoons[r_1(x)]{r_0(x)} 1. \quad (2)$$

While the microscopic interpretation of y is uncertain, we conjecture that it represents a slow configurational degree of freedom that determines whether a hopper with no net flow will clog permanently or pause temporarily. With the addition of the hidden variable, $x = y = 0$ is an absorbing state of the dynamics, i.e. the clog state, while $x \approx 0, y = 1$ represents a pause. During a pause, the system is susceptible to noise ϵ that perturbs the flow-rate dynamics, Eq. (1), and allows steady flow to resume. Since spontaneous unclogging is possible even in the absence of vibrations [25, 26, 33], this additive noise has contributions both intrinsic to the system and from external vibrations.

The hidden variable switching rates satisfy $r_0(0) = 0$ to preserve the absorbing clog state. Expanding to linear order in x (assuming no transitions occur when $x < 0$ [39]), we have $r_0(x) = (r_0 \cdot x/x_0)\theta(x)$ and $r_1(x) = (r_{1,0} + r_1 \cdot x/x_0)\theta(x)$, where $\theta(x)$ is the Heaviside theta function and x_0 is the steady flow rate. If $r_{1,0}$ is too large, direct transitions from pause to clog frequently occur and unpausing events would not be observed in experiments. Therefore, we assume $r_{1,0} = 0$, but our results are robust for $(r_{1,0})^{-1} \gg \tau_P$, the average pause duration. Simulated trajectories of the stochastic model closely resemble the experimental flows as do the corresponding flow-rate distributions [Fig. 1(c)].

We can represent the granular flow dynamics using an even simpler four-state model [Fig. 2(a)]: two indistinguishable flow states F_0 and F_1 , a pause state P , and a clog state C . During steady flow, the system switches between the flow states based on the dynamics of the hidden variable y ; the balance between these states, r_1/r_0 , determines the likelihood of clogging versus pausing. The

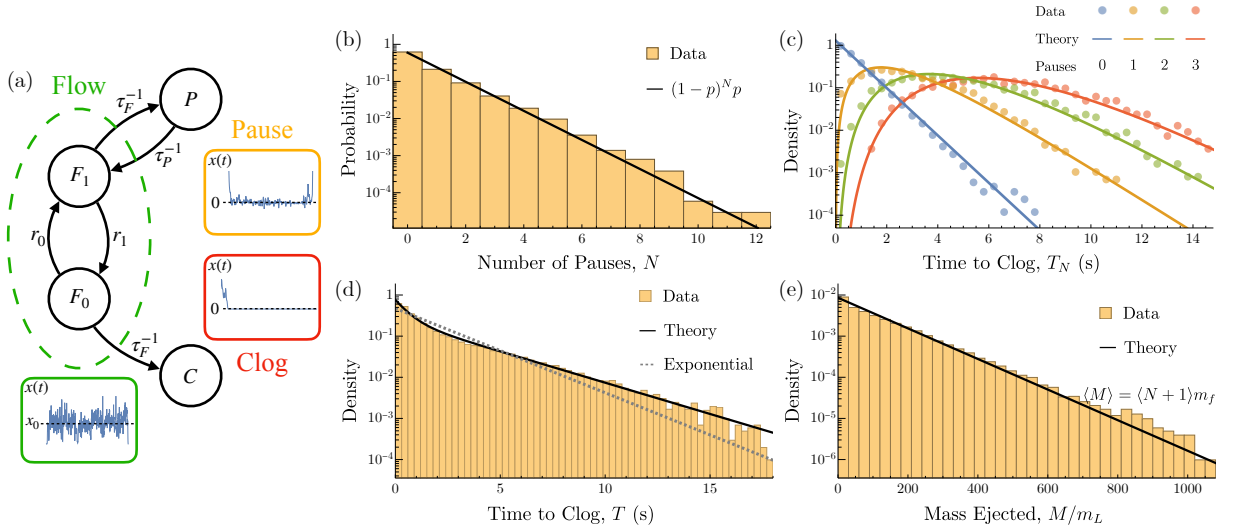


FIG. 2. *Statistical predictions of the four-state model.* (a) A four-state model of granular flows. Two flow states F_0 and F_1 (corresponding to the states of the hidden variable, $y = 0, 1$) determine whether the system will pause P or clog C when the flow rate fluctuates toward zero. The boxes show flow-rate trajectories that correspond to each of these coarse-grained states. (b) The number of pauses is geometrically distributed with $\langle N \rangle = 0.682$. (c) Distributions of clog times for trajectories with a given number of pauses before the final clog. Solid lines are the prediction Eq. (4). (d) Distribution of clog times across all trajectories. Lines show an exponential fit (dashed) and the predicted distribution (solid) Eq. (5). The exponential time scales are $\tau_+ = 2.856$ s and $\tau_- = 0.580$ s with $c = 0.301$. (e) The total ejected mass M is exponentially distributed with mean $\langle N + 1 \rangle m_F = 116.7 m_L$. Model parameters p , τ_F , τ_P and m_F are fit in (b) and [38]; the predictions in (c)-(e) require no fitting. All data are from the $D = 3.86 d_L$ dataset.

flow preceding a pause or clog has average lifetime τ_F and pauses have lifetime τ_P . In our experiments flow and pause duration are exponentially distributed, at least for short times, with $\tau_F = 0.77$ s and $\tau_P = 1.26$ s [38].

The four-state model accurately predicts the statistics of the number of pauses before clogging. If the switching of the hidden variable is fast compared to the flow duration, then as the flow rate fluctuates toward zero it will clog with probability $p = r_1/(r_0 + r_1)$ and pause with probability $1 - p = r_0/(r_0 + r_1)$. The number of pauses N before a permanent clog are geometrically distributed,

$$p(N) = (1 - p)^N p, \quad \langle N \rangle = \frac{1 - p}{p}. \quad (3)$$

Fig 2(b) shows the number of pauses in the measured flow trajectories are indeed geometric, with $p = 0.595$ or $\langle N \rangle = 0.682$. When the flow rate fluctuates toward zero, it clogs or pauses (with probability p and $1 - p$ respectively) depending on the state of the hidden variable. Each of these outcomes over the duration of the entire flow are independent.

With the measured clog probability p and timescales τ_F and τ_P [38], we use the model to predict (with no additional fitting) the distribution of the total time to clog T and the distribution of clogging time T_N for flows with exactly N pauses. Starting with the latter, T_N is the sum of N pauses and $N+1$ flows, $T_N = \tau_F^0 + \sum_{i=1}^N \tau_F^i + \tau_P^i$, where $\tau_{F/P}^i$ are exponentially distributed flow and pause

durations, $\tau_{F/P}^i \sim \mathcal{E}_{F/P}(t) = \tau_{F/P}^{-1} \exp(-t/\tau_{F/P})$. Given that a trajectory has N pauses, the distribution of flow times is [38],

$$p_{T_N}(t) = \frac{\sqrt{\pi}}{2N!} \frac{t^{N+1/2} \mathcal{T}^{N-1/2}}{\tau_F^{N+1} \tau_P^N} \exp\left(-\frac{t(\tau_F + \tau_P)}{2\tau_F \tau_P}\right) \times \left[I_{N-1/2}\left(\frac{t}{2\mathcal{T}}\right) - I_{N+1/2}\left(\frac{t}{2\mathcal{T}}\right) \right] \quad (4)$$

where $I_\alpha(x)$ is the modified Bessel Function of the first kind and $\mathcal{T} = \tau_P \tau_F / (\tau_P - \tau_F)$. Fig. 2(c) shows this prediction with no fit parameters excellently captures the measured clogging-time distributions, conditioned on number of pauses N .

To obtain the clogging-time distribution p_T for the entire ensemble of measured flows, we average $p_{T_N}(t)$ over the geometric distribution Eq. (3), $p_T(t) = \sum_{N=0}^{\infty} p_{T_N}(t) p(1 - p)^N$. The resulting distribution is

$$p_T(t) = \frac{c}{\tau_+} e^{-t/\tau_+} + \frac{(1 - c)}{\tau_-} e^{-t/\tau_-}, \quad (5)$$

where the exponential time-scales are given by $\tau_{\pm} = 2\tau_F \tau_P / (\tau_F + \tau_P \mp \tilde{\tau})$ with relative weighting $c = 1/2 + [(1 - 2p)\tau_P + \tau_F] / \tilde{\tau}$ and $\tilde{\tau} = \sqrt{(\tau_F + \tau_P)^2 - 4p\tau_F \tau_P}$. The predicted double exponential distribution, Eq. (5), captures the data noticeably better than a single exponential [Fig. 2(d)]. We find that τ_F increases with outlet size D , while τ_P is approximately constant [38]. For large

outlets ($\tau_F \gg \tau_P$), the competing time scales become $c\tau_+ \approx \tau_F/p$ and $(1-c)\tau_- \approx p(1-p)\tau_P^3/\tau_F^2$, with the former dominating to recover the established exponentially distributed clogging time in this regime [3, 17, 18, 22, 40].

In contrast to the clogging time, we predict that the mass ejected before clogging M is exponential, consistent with experiments [Fig. 2(e)]. If m_F is the mean mass ejected during a flow (no mass is ejected during a pause), the mass ejected in a trajectory with N pauses is $M_N = \sum_{i=0}^N m_F^i$, which follows a Gamma distribution, Gamma($N+1, m_F$). Averaging over the geometric number of pauses produces an exponential distribution with predicted mean $\langle M \rangle = m_F \langle N+1 \rangle = 116.7m_L$, within 2% of the empirical average mass ejected.

The full Langevin model, Eqs. (1) and (2), provides deeper insight into the flow rate statistics. The distribution of flow rates $P_y(x, t)$ for the hidden variable state $y = 0, 1$ satisfy a coupled Fokker-Planck equation (using the Itô interpretation for multiplicative noise),

$$\frac{\partial P_y}{\partial t} = -\frac{\partial(fP_y)}{\partial x} + \frac{\partial^2(g_y P_y)}{\partial x^2} + \mathcal{R}(y \rightarrow 1-y) \quad (6)$$

where $g_y(x) = g(x) + \epsilon y$ includes background noise when $y = 1$ and $\mathcal{R}(y \rightarrow 1-y) = \frac{x}{x_0}(r_{1-y}P_{1-y} - r_y P_y)\theta(x)$ describes the flow of probability between P_0 and P_1 from the dynamics of the hidden variable. The measured flow-rate distributions are well approximated by the slowest decaying mode of the Fokker-Planck operator \mathcal{L}_{FP} . We compute this eigenfunction numerically and fit to experiments by tuning the noise $\Delta\tau_0$, steady flow-rate x_0 , and two additional parameters that capture nonlinear deformations of the force [38].

The fit distributions for various outlet sizes and the corresponding effective potentials $\Phi(x) = -\int [f(x) - g'(x)]/g(x) dx$ are shown in Fig. 3. Intuitively, the larger outlet size promotes faster flows (larger x_0). The noise grows, approximately proportionally to x_0 , but larger outlets have smaller relative fluctuations ($\tilde{\Delta} = \Delta\tau_0/x_0^2$ shrinks). Our model explains both the non-Gaussian shape and the peak near zero that appear in small outlet flow-rate distributions. The former arises due to the larger fluctuations and proximity of the steady flow rate x_0 to the clog state $x = 0$, while the latter comes from coupling to the hidden mode y .

Finally, via first-passage-time analysis, we predict the asymptotic scaling of the clogging time for large outlets [38, 41]: $\langle T \rangle \approx \tau_F/p \sim \tau_0 p^{-1} C \exp(c\tilde{\Delta}^{-1})$. From fitting the flow-rate distributions, the relative noise decays as the square of the outlet size $\tilde{\Delta} \propto D^{-2}$ [Fig. 3(b), inset]. Remarkably, combining these scaling laws produces the previously measured stretched-exponential growth of the clogging time [21, 22, 26, 40], $\langle T \rangle \propto \exp(cD^\alpha)$, where α is the dimension of the hopper ($\alpha = 2$ in our experiment). This result provides further theoretical basis for the apparent lack of a critical clogging transition as outlet size increases [21, 26]. Furthermore, the effective

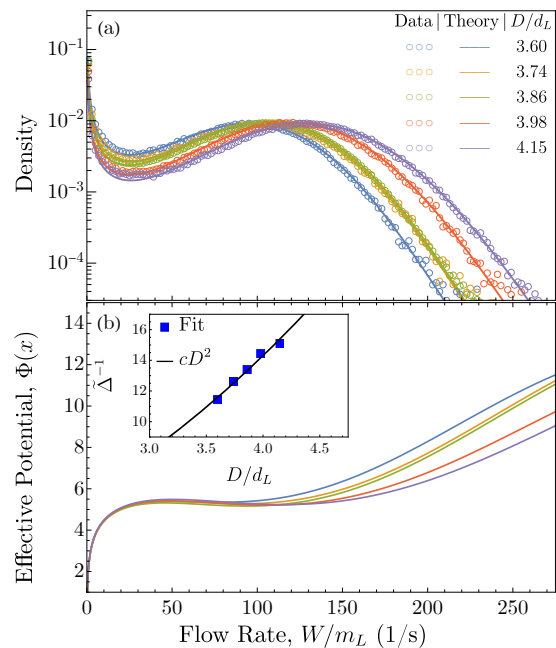


FIG. 3. (a) Measured (symbols) and fit (lines) flow-rate distributions for various outlet sizes. (b) The corresponding effective potentials $\Phi(x)$ and (inset) D -dependence of $\tilde{\Delta} = \Delta\tau_0/x_0^2$ from fit parameters x_0 and $\Delta\tau_0$, which scales quadratically $\tilde{\Delta}^{-1} = 0.89(D/d_L)^2$.

noise $\tilde{\Delta} \sim N_{\text{outlet}}^{-1}$, scales with the number of grains in the outlet: the multiplicative noise term arises due to the discrete nature of the small number of grains whose configurations determine the flow rate.

To summarize, the statistics of granular flows can be described entirely in terms of the Langevin dynamics of the flow rate, driven by multiplicative noise and coupled to a slow hidden mode that controls clog stability. Our minimal model explains the emergence of intermittent pauses for small outlets, as well as the non-exponential statistics of clogging times and the non-Gaussian instantaneous flow rate. The Markovian nature of the flow rate dynamics means the current state provides little information for clog prediction. For example, in our model when the flow rate is 10% of x_0 there is only a 75% chance of an imminent clog [38]. However, if one could predict clogs by external means, monitoring the hidden variable would provide advance notice of whether the incipient clog will be temporary or permanent [38].

Looking forward, an important question will therefore be the microscopic nature of the hidden variable identified in this study. Our work constrains the timescales of its dynamics: they are slower than the flow-rate correlation time but faster than the flow duration ($\tau_0^{-1} \gg r_0, r_1 \gg \tau_F^{-1}$). Previous work offers further hints: slow relaxation of grains in upper layers of the silo have been observed during pauses [33]. Can we identify a measurable order parameter that quantifies this behavior, not

only during pauses, but also during steady flow? Applying machine learning algorithms to snapshots of granular flows has recently seen success in classifying clog-causing configurations [34]. Perhaps this approach can distinguish between metastable and permanent clogs and will enable tracking of the hidden variable throughout a flow trajectory.

More generally, our phenomenological model should apply across a broad range of outlet sizes and vibration amplitudes. For example, at small enough D we anticipate a saddle-node bifurcation in the effective potential, where the stable flow state vanishes. Here the clogging statistics will become distinctly non-exponential and exhibit universal scaling [42]. Increasing vibrations pushes granular flows through a critical transition, beyond which permanent clogging is impossible [23]. Our model should naturally extend to this case, through vibrational dependence in the additive noise and other parameters. Understanding the dynamics underlying this transition will shed further light on the fundamental requirements for clogging.

This work was partially supported by NSF grants MRSEC/DMR-1720530 and MRSEC/DMR-2309043. D.J.D. and Y.T. thank the Aspen Center for Physics, which is supported by NSF grant PHY-2210452. D.J.D. thanks CCB at the Flatiron Institute, a division of the Simons Foundation, as well as the Isaac Newton Institute for Mathematical Sciences under the program “New Statistical Physics in Living Matter” (EPSRC grant EP/R014601/1), for support and hospitality while a portion of this research was carried out. S.D. acknowledges support from the University of Pennsylvania School of Arts and Sciences Data Driven Discovery Initiative.

-
- [1] S. S. Manna and H. J. Herrmann, Intermittent granular flow and clogging with internal avalanches, *European Physical Journal E* **1**, 341 (2000).
- [2] K. To, P. Y. Lai, and H. K. Pak, Jamming of granular flow in a two-dimensional hopper, *Physical Review Letters* **86**, 71 (2001).
- [3] I. Zuriguel, A. Garcimartín, D. Maza, L. Pagnaloni, and J. Pastor, Jamming during the discharge of granular matter from a silo, *Physical Review E* **71**, 051303 (2005).
- [4] I. Zuriguel, D. R. Parisi, R. C. Hidalgo, C. Lozano, A. Janda, P. A. Gago, J. P. Peralta, L. M. Ferrer, L. A. Pagnaloni, E. Clément, D. Maza, I. Pagonabarraga, and A. Garcimartín, Clogging transition of many-particle systems flowing through bottlenecks., *Scientific reports* **4**, 7324 (2014).
- [5] N. Roussel, T. L. H. Nguyen, and P. Coussot, General probabilistic approach to the filtration process, *Phys. Rev. Lett.* **98**, 114502 (2007).
- [6] A. Marin, H. Lhuissier, M. Rossi, and C. J. Kähler, Clogging in constricted suspension flows, *Phys. Rev. E* **97**, 021102 (2018).
- [7] R. L. Stoop and P. Tierno, Clogging and jamming of colloidal monolayers driven across disordered landscapes, *Communications Physics* **1**, 68 (2018).
- [8] M. Souzy, I. Zuriguel, and A. Marin, Transition from clogging to continuous flow in constricted particle suspensions, *Phys. Rev. E* **101**, 060901 (2020).
- [9] E. Dressaire and A. Sauret, Clogging of microfluidic systems, *Soft Matter* **13**, 37 (2017).
- [10] A. L. Fogelson and K. B. Neeves, Fluid mechanics of blood clot formation, *Annual Review of Fluid Mechanics* **47**, 377 (2015).
- [11] K. Drescher, Y. Shen, B. L. Bassler, and H. A. Stone, Biofilm streamers cause catastrophic disruption of flow with consequences for environmental and medical systems, *Proceedings of the National Academy of Sciences* **110**, 4345 (2013).
- [12] D. Helbing, I. Farkas, and T. Vicsek, Simulating dynamical features of escape panic, *Nature* **407**, 487 (2000).
- [13] D. Helbing, L. Buzna, A. Johansson, and T. Werner, Self-organized pedestrian crowd dynamics: Experiments, simulations, and design solutions, *Transportation Science* **39**, 1 (2005).
- [14] A. Hafez, Q. Liu, T. Finkbeiner, R. A. Alouhali, T. E. Moellendick, and J. C. Santamarina, The effect of particle shape on discharge and clogging, *Scientific Reports* **11**, 3309 (2021).
- [15] D. Gella, D. Yanagisawa, R. Caitano, M. V. Ferreyra, and I. Zuriguel, On the dual effect of obstacles in preventing silo clogging in 2d, *Communications Physics* **5**, 4 (2022).
- [16] F. G. Escudero Acuña, M. C. Villagrán Olivares, J. G. Benito, and A. M. Vidales, Kinematics of the discharge of flat particles from model silos, *Granular Matter* **24**, 102 (2022).
- [17] I. Zuriguel, A. Janda, A. Garcimartín, C. Lozano, R. Arévalo, and D. Maza, Silo Clogging Reduction by the Presence of an Obstacle, *Physical Review Letters* **107**, 278001 (2011).
- [18] C. C. Thomas and D. J. Durian, Geometry dependence of the clogging transition in tilted hoppers, *Physical Review E* **87**, 052201 (2013).
- [19] I. Zuriguel and A. Garcimartín, Statistical mechanics of clogging, in *Encyclopedia of Complexity and Systems Science*, edited by R. A. Meyers (Springer Berlin Heidelberg, Berlin, Heidelberg, 2020) pp. 1–32.
- [20] A. Janda, I. Zuriguel, and D. Maza, Flow Rate of Particles through Apertures Obtained from Self-Similar Density and Velocity Profiles, *Phys. Rev. Lett.* **108**, 248001 (2012).
- [21] C. C. Thomas and D. J. Durian, Fraction of Clogging Configurations Sampled by Granular Hopper Flow, *Physical Review Letters* **114**, 178001 (2015).
- [22] A. Janda, I. Zuriguel, A. Garcimartín, L. A. Pagnaloni, and D. Maza, Jamming and critical outlet size in the discharge of a two-dimensional silo, *EPL (Europhysics Letters)* **84**, 44002 (2008).
- [23] R. Caitano, B. V. Guerrero, R. E. R. González, I. Zuriguel, and A. Garcimartín, Characterization of the clogging transition in vibrated granular media, *Phys. Rev. Lett.* **127**, 148002 (2021).
- [24] P. A. Gago, M. A. Madrid, S. Boettcher, R. Blumenfeld, and P. King, Effect of bevelled silo outlet in the flow rate during discharge, *Powder Technology* **428**, 118842 (2023).
- [25] A. Janda, R. Harich, I. Zuriguel, D. Maza, P. Cixous, and

- A. Garcimartín, Flow-rate fluctuations in the outpouring of grains from a two-dimensional silo, *Phys. Rev. E* **79**, 031302 (2009).
- [26] C. C. Thomas and D. J. Durian, Intermittency and velocity fluctuations in hopper flows prone to clogging, *Phys. Rev. E* **94**, 022901 (2016).
- [27] S. Zhang, Z. Zeng, H. Yuan, Z. Xu, X. Ai, L. He, Z. Li, and Y. Wang, Experimental study of granular clogging in two-dimensional hopper, *arXiv preprint arXiv:2308.06584* (2023).
- [28] A. Janda, D. Maza, A. Garcimartín, E. Kolb, J. Lanuza, and E. Clément, Unjamming a granular hopper by vibration, *Europhysics Letters* **87**, 24002 (2009).
- [29] C. Merrigan, S. K. Birwa, S. Tewari, and B. Chakraborty, Ergodicity breaking dynamics of arch collapse, *Phys. Rev. E* **97**, 040901 (2018).
- [30] A. Nicolas, A. Garcimartín, and I. Zuriguel, Trap model for clogging and unclogging in granular hopper flows, *Phys. Rev. Lett.* **120**, 198002 (2018).
- [31] B. V. Guerrero, B. Chakraborty, I. Zuriguel, and A. Garcimartín, Nonergodicity in silo unclogging: Broken and unbroken arches, *Phys. Rev. E* **100**, 032901 (2019).
- [32] Y. Bertho, F. Giorgiutti-Dauphiné, and J.-P. Hulin, Intermittent dry granular flow in a vertical pipe, *Phys. Fluids* **15**, 3358 (2003).
- [33] K. Harth, J. Wang, T. Börzsönyi, and R. Stannarius, Intermittent flow and transient congestions of soft spheres passing narrow orifices, *Soft Matter* **16**, 8013 (2020).
- [34] J. M. Hanlan, S. Dillavou, A. J. Liu, and D. J. Durian, Cornerstones are the key: Using interpretable machine learning to probe clogging in granular hoppers, in preparation (2023).
- [35] G. Grinstein, M. A. Muñoz, and Y. Tu, Phase structure of systems with multiplicative noise, *Phys. Rev. Lett.* **76**, 4376 (1996).
- [36] M. A. Muñoz, G. Grinstein, and Y. Tu, Survival probability and field theory in systems with absorbing states, *Phys. Rev. E* **56**, 5101 (1997).
- [37] We also fit forces of the form $f(x) \propto (x - x_0)(Ax + Bx^2)$. In all cases the quadratic term was dominant and including the linear term does not considerably reduce the fitting loss.
- [38] See Supplemental Material at for additional data, details of mathematical derivations, and fitting procedures.
- [39] Negative flow rate is observed in the experiment due to particles being pushed upward across the mass boundary line [see Fig. 1(a)]. Allowing negative flow and transitions for $x < 0$ in the model only changes the flow rate distribution at very small and negative x without impacting other results significantly.
- [40] K. To, Jamming transition in two-dimensional hoppers and silos, *Phys. Rev. E* **71**, 060301 (2005).
- [41] N. G. van Kampen, *Stochastic processes in physics and chemistry* (Elsevier, Amsterdam, 2007).
- [42] D. Hathcock and J. P. Sethna, Reaction rates and the noisy saddle-node bifurcation: Renormalization group for barrier crossing, *Phys. Rev. Res.* **3**, 013156 (2021).

Supplemental Material for “Stochastic dynamics of granular hopper flows: hidden modes control the stability of clogs”

David Hathcock,¹ Sam Dillavou,² Jesse M. Hanlan,² Douglas J. Durian,² and Yuhai Tu¹

¹*IBM T. J. Watson Research Center, Yorktown Heights, NY 10598, USA*

²*Department of Physics & Astronomy, University of Pennsylvania, Philadelphia, PA 19104, USA*

(Dated: October 5, 2024)

S1. CLOG STATISTICS IN THE FOUR-STATE MODEL

A. Distribution of the flow duration with N pauses

As noted in the main text, the total time before clogging, given the trajectory has exactly N pauses is given by

$$T_N = \tau_F^0 + \sum_{i=1}^N \tau_F^i + \tau_P^i, \quad (\text{S1})$$

where τ_F^i and τ_P^i denote the duration of each flow and pause, which are exponentially distributed with mean $\tau_{F/P}$: $\tau_{F/P}^i \sim \mathcal{E}_{F/P}(t) = \tau_{F/P}^{-1} \exp(-t/\tau_{F/P})$. The resulting distribution for T_N is given by a convolution of these exponential distributions,

$$\begin{aligned} p_{T_N}(t) &= \underbrace{\mathcal{E}_F(t) * \mathcal{E}_F(t) * \dots * \mathcal{E}_F(t)}_{N+1 \text{ times}} * \underbrace{\mathcal{E}_P(t) * \dots * \mathcal{E}_P(t)}_{N \text{ times}} = \text{Gamma}(N+1, \tau_F) * \text{Gamma}(N, \tau_P) \\ &= \int_0^t \frac{s^N}{N! \tau_F^{N+1}} e^{-s/\tau_F} \cdot \frac{(t-s)^{N-1}}{(N-1)! \tau_P^N} e^{-(t-s)/\tau_P} ds. \end{aligned} \quad (\text{S2})$$

Here $*$ denotes the convolution, which is written out explicitly in the second line. We use the fact that the sum of N identically distributed exponential random variables follows a Gamma distribution. Note that the integration limits are finite because the Gamma distribution is zero for negative times. To evaluate the convolution, we separate the integrand into three terms,

$$p_{T_N} = \int_0^t \frac{e^{-t/t_P - s/\mathcal{T}}}{N!(N-1)! \tau_F^{N+1} \tau_P^N} \left[\frac{t}{2} s^{N-1} (t-s)^{N-1} - \frac{1}{2N\mathcal{T}} s^N (t-s)^N + \frac{s^{N-1} (t-s)^{N-1} [N\mathcal{T}(2s-t) + s(t-s)]}{2N\mathcal{T}} \right], \quad (\text{S3})$$

where $\mathcal{T} = \tau_P \tau_F / (\tau_P - \tau_F)$. The final term integrates to: $\exp(-s/\mathcal{T}) s^N (t-s)^N / (2N) \Big|_{s=0}^{s=t} = 0$. The first two terms can be expressed in terms of the modified Bessel function of the first kind $I_\alpha(x)$, leading to

$$p_{T_N}(t) = \frac{\sqrt{\pi}}{2N!} \frac{t^{N+1/2} \mathcal{T}^{N-1/2}}{\tau_F^{N+1} \tau_P^N} \exp\left(-\frac{t(\tau_F + \tau_P)}{2\tau_F \tau_P}\right) \left[I_{N-1/2}\left(\frac{t}{2\mathcal{T}}\right) - I_{N+1/2}\left(\frac{t}{2\mathcal{T}}\right) \right], \quad (\text{S4})$$

which is the final result quoted in the main text, Eq. (4). The first few distributions are,

$$\begin{aligned} p_{T_0}(t) &= \tau_F^{-1} e^{-t/\tau_F}, \\ p_{T_1}(t) &= \frac{\mathcal{T}^2}{\tau_F^2 \tau_P} e^{-t/\tau_P} - \frac{t\mathcal{T} + \mathcal{T}^2}{\tau_F^2 \tau_P} e^{-t/\tau_F}, \\ p_{T_2}(t) &= \frac{t\mathcal{T}^3 - 3\mathcal{T}^4}{\tau_F^3 \tau_P} e^{-t/\tau_P} + \frac{t^2\mathcal{T}^2 + 4t\mathcal{T}^3 + 6\mathcal{T}^4}{2\tau_F^3 \tau_P^2} e^{-t/\tau_F}. \end{aligned} \quad (\text{S5})$$

B. Ensemble distribution of the flow duration

The distribution of flow duration across the entire ensemble of flow trajectories is given by $p_{T_N}(t)$ averaged over the the geometric distribution for the number of pauses $p(N) = p(1-p)^N$,

$$p_T(t) = \sum_{N=0}^{\infty} p_{T_N}(t)p(1-p)^N. \quad (\text{S6})$$

As in the main text, $p = r_1/(r_0+r_1)$ is the probability of clogging when the flow rate fluctuates toward zero (r_i are the switching rates for the hidden variable). This average can be computed in Fourier space. Defining the Fourier transform $f(\omega) = \mathcal{F}[f(t)] = \int_{-\infty}^{\infty} dt f(t) \exp(i\omega t)$, the transformed exponential distributions are $\mathcal{E}_{F/P}(\omega) = 1/(1-i\omega\tau_{F/P})$. After Fourier transforming, the convolution in Eq. (S2) becomes a product,

$$\begin{aligned} p_T(\omega) &= \sum_{N=0}^{\infty} \frac{1}{(1-i\omega\tau_F)^{N+1}} \frac{1}{(1-i\omega\tau_P)^N} p(1-p)^N \\ &= \frac{p(1-i\tau_P\omega)}{p-i\omega(\tau_F+\tau_P)-\tau_F\tau_P\omega} \end{aligned} \quad (\text{S7})$$

Taking the inverse Fourier transform leaves us with the distribution quoted in the main text [Eq. (5)],

$$p_T(t) = \frac{c}{\tau_+} e^{-t/\tau_+} + \frac{(1-c)}{\tau_-} e^{-t/\tau_-}, \quad (\text{S8})$$

where τ_{\pm}^{-1} are the poles of Eq. (S7)

$$\tau_{\pm} = \frac{2\tau_F\tau_P}{\tau_F + \tau_P \pm \sqrt{(\tau_F + \tau_P)^2 - 4p\tau_F\tau_P}} \quad (\text{S9})$$

and the relative weighting c is given by,

$$c = \frac{1}{2} + \frac{(2p-1)\tau_P - \tau_F}{2\sqrt{(\tau_F + \tau_P)^2 - 4p\tau_F\tau_P}}. \quad (\text{S10})$$

C. Distribution of mass ejected

As mentioned in the main text, because no mass is ejected during the pauses, the total mass ejected over the duration of the entire flow remains exponentially distributed. Following the calculations in the preceding sections, we assume m_F is the average mass ejected during each flow (preceding a pause or clog). Then the mass ejected in a flow with N pauses is $M_N = \sum_{i=0}^N m_F^i$; again we assume m_F^i are exponentially distributed, $m_F^i \sim \mathcal{E}_M(m) = m_F^{-1} \exp(m/m_F)$. It follows that the distribution of mass ejected (given N pauses) is

$$p_{M_N}(m) = \underbrace{\mathcal{E}_M(m) * \mathcal{E}_M(m) * \dots * \mathcal{E}_M(m)}_{N+1 \text{ times}} = \text{Gamma}(N+1, m_F). \quad (\text{S11})$$

The distribution of mass ejected across all trajectories is (in Fourier space),

$$p_M(\omega) = \sum_{N=0}^{\infty} \frac{1}{(1-i\omega m_F)^{N+1}} p(1-p)^N = \frac{1}{1-i\omega m_F/p}, \quad (\text{S12})$$

which corresponds to an exponential distribution with mean $m_F/p = m_F \langle N+1 \rangle$ (the number of flows is one more than the number of pauses), as quoted in the main text.

S2. ADDITIONAL DATA: FLOW AND PAUSE TIMESCALES, MASS EJECTED, AND OUTLET-SIZE DEPENDENCE

The four-state model calculations in the preceding sections assume that the flow duration and mass ejected preceding a clog or pause as well as the pause duration are each exponentially distributed. Fig. S1(a) shows that the flow duration

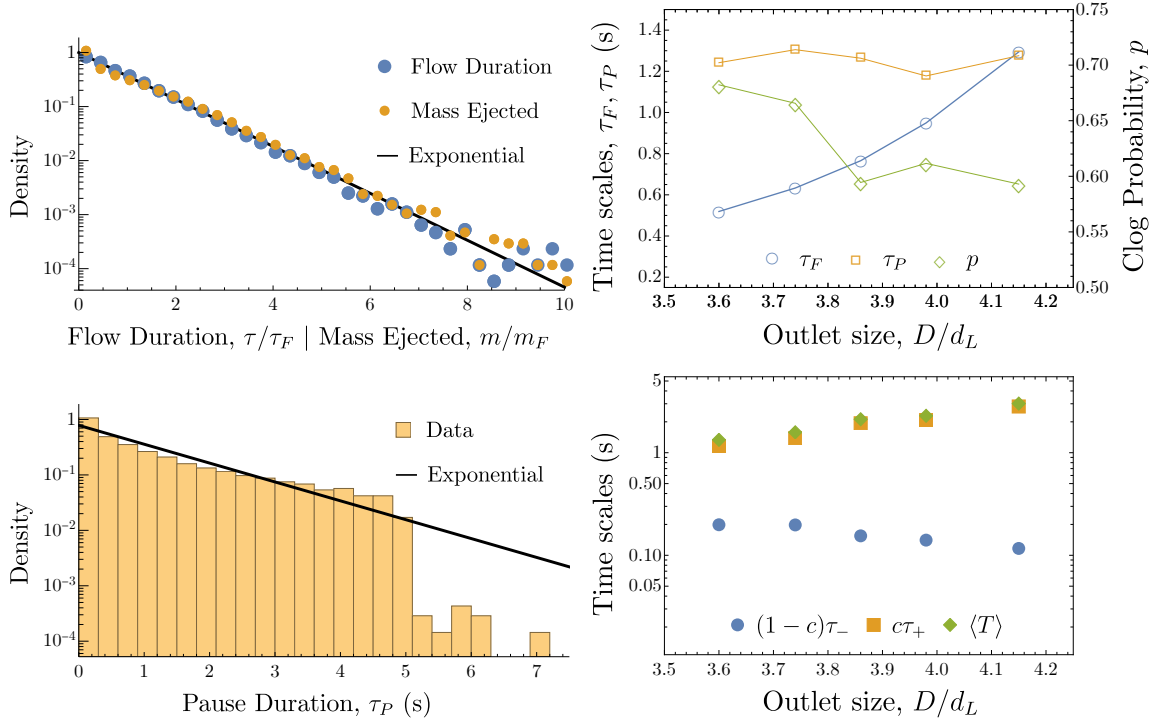


FIG. S1. *Time scales, mass ejected, and outlet-size dependence.* (a) The distributions of flow duration and mass ejected before each pause or clog (normalized by their respective means $\tau_F = 0.77\text{s}$ and $m_F = 69.4m_L$). Each closely follow an exponential distribution. (b) Distribution of pause duration. Note that long pauses ($\gtrsim 5\text{s}$) are cut off due to the criteria for identifying clogs during automated data collection. The solid line is exponential fit with mean $\tau_P = 1.26\text{s}$, adjusted to account for the cutoff. Data in (a-b) are from the $D = 3.86d_L$ dataset. (c) Outlet size dependence of the average flow and pause timescales τ_F and τ_P and the clog probability p . (d) Outlet size dependence of the clogging timescales in Eq. (S8) that contribute to the mean $\langle T \rangle = c\tau_+ + (1-c)\tau_-$. For larger outlets the single timescale $c\tau_+$ becomes increasingly dominant.

and mass ejected before each pause or clog do closely follow an exponential distribution (with means $\tau_F = 0.77\text{s}$ and $m_F = 69.4m_L$ respectively). The pause duration also appears to be exponential [Fig. S1(b)], at least at short times. In this distribution, long-lived pauses $\gtrsim 5\text{s}$ are cutoff because they are classified as permanent clogs during the automated data collection. Previous work on vibrated granular systems suggests the tail of the pause-distribution decays as a power-law [1–4], with exponent decreasing with vibration amplitude. In these studies, however, the power-law scaling is only satisfied for very large and rare pause times that accounting for less than 1/100 to 1/10 pauses depending on experimental conditions. Thus we expect that the exponential approximation will be suitable for capturing statistics of all trajectories except those with very long pauses.

The predictions shown in Fig. 2 of the main text [Eqs. (S4), (S8), and (S12)] also hold across each of the outlet sizes in our dataset $D/d_L = 3.6, 3.74, 3.86, 3.98, \text{ and } 4.15$. Fig. S1(c) shows how the empirical flow and pause timescales τ_F and τ_P as well as the clog probability p vary with outlet size. Unsurprisingly, the flow duration τ_F increases and the clog probability p decreases with outlet size. When the outlet is larger, it takes longer to form an arch and these arches are more susceptible to spontaneous declogging. The pause duration τ_P is approximately constant with outlet size, though we expect it will decrease if the outlet is large enough; again, arches tend to be less stable when the outlet is larger.

Fig. S1(d) shows the contribution of the two timescales in Eq. (S8), to the mean total clogging time, $\langle T \rangle = c\tau_+ + (1-c)\tau_-$. As the outlet size increases, the first time-scale becomes increasingly dominant ($\langle T \rangle \approx c\tau_+$ and non-exponential features of the clog time diminish. As mentioned in the main text, the increase in τ_F in Fig. S1(c) implies this behavior: for $\tau_F \gg \tau_P$ we have $c\tau_+ \approx \tau_F/p$ and $(1-c)\tau_- \approx p(1-p)\tau_P^3/\tau_F^2$, the first of which is dominant.

S3. FITTING AND ANALYSIS OF THE FOKKER-PLANCK EQUATION

In this section we describe the flow-rate distribution fits and analytical results following from the Fokker-Planck equation for our hidden variable model [Eq. (6) in the main text]. Writing out the dependence on the hidden variable

state $y = 0, 1$ explicitly, the Fokker-Planck equation is given by,

$$\begin{aligned}\frac{\partial P_0}{\partial t} &= -\frac{\partial}{\partial x}(fP_0) + \frac{\partial^2}{\partial x^2}(gP_0) + \frac{x}{x_0}(r_1P_1 - r_0P_0)\theta(x) \\ \frac{\partial P_1}{\partial t} &= -\frac{\partial}{\partial x}(fP_0) + \frac{\partial^2}{\partial x^2}((g + \epsilon)P_0) + \frac{x}{x_0}(r_0P_0 - r_1P_1)\theta(x),\end{aligned}\tag{S13}$$

where $\theta(x)$ is the Heaviside function. Since there is an absorbing state for $y = 0$, $P_0(x)$ is defined for $x > 0$, while $P_1(x)$ is defined for all x . The final term in these equations captures the flow of probability between P_0 and P_1 based on the dynamics of the hidden variable y . We denote the coupled Fokker-Planck operator by \mathcal{L}_{FP} : $\partial\mathbf{P}/\partial t = \mathcal{L}_{\text{FP}}\mathbf{P}$, where $\mathbf{P} = \{P_0, P_1\}$.

A. Deterministic force and flow-rate distribution fitting

The time-dependent flow-rate distributions can be expanded as, $\mathbf{P}(x, t) = \sum_{i=0}^{\infty} a_i \exp(-\lambda_i t)\mathbf{P}^i(x)$, in terms of eigenfunctions $\mathbf{P}^i(x)$ and corresponding eigenvalues $-\lambda_i$ of the Fokker-Planck operator: $\mathcal{L}_{\text{FP}}\mathbf{P}^i(x) = -\lambda_i\mathbf{P}^i(x)$. The constants a_i are determined by the initial distribution and the eigenvalues are ordered: $0 < \lambda_0 < \lambda_1 < \dots$, so that $\mathbf{P}^0(x)$ is the slowest decaying mode. Assuming a separation of time-scales $\lambda_0 \ll \lambda_1$, the distribution of clog times is exponential $p_T(t) \approx \lambda_0 \exp(-\lambda_0 t)$, which is consistent with our measurements except at short times [main text, Fig. 2(d)]. The measured flow-rate distribution is then well approximated by the sum of the components of the slowest decaying mode $P_0^0(x) + P_1^0(x)$. All higher-order eigenfunctions quickly decay and the clogging process is dominated by the exponential decay of this single mode.

To compute and fit the leading eigenfunction to measured flow-rate distributions, we discretize the Fokker-Planck operator \mathcal{L}_{FP} over a range of x that is much larger than all measured flow rates. We use the force,

$$f(x) = -\frac{(x - x_0)x^2}{\tau_0 x_0^2} \cdot \frac{x^2 - 2ax + a^2 + b^2}{x_0^2 - 2ax_0 + a^2 + b^2},\tag{S14}$$

which has roots at x_0 and 0 that respectively correspond to the steadily flowing state and the clogged state. The later is taken to be quadratic, so that the clogged state is stable to negative perturbations (flow upward in the hopper), but unstable to positive perturbations (that re-initiate the flow). We also fit forces of the form $f(x) \propto (x - x_0)(Ax + Bx^2)$, but the quadratic term was always dominant and including the linear term does not considerably reduce the fitting loss. The second term in Eq. (S14) (denoted $\Psi(x)$ in the main text) is positive-definite, allowing for deformation of the potential without introducing new extrema. The factors in the denominator fix the units; τ_0 is the harmonic decay time near x_0 .

Using Eq. (S14) for the force and linear noise $g(x) = \Delta x/x_0$, fitting flow-rate distributions involves tuning 4 parameters $x_0, a, b, \Delta\tau_0$ (the eigenfunction is independent of the overall time-scale). To fix the scale of Δ and τ_0 , we match the autocorrelation time of the flow rate trajectories to that obtained from simulations, finding $\tau_0 \approx 20 - 22$ ms with no clear dependence on D over this range of outlet-sizes. We also fix $p = r_1/(r_0 + r_1)$ to match the measured geometric pause statistics and choose $r_0 = (10\tau_0)^{-1}$ so that the switching time-scale for y is slower than the flow-rate correlation time but faster than the flow and pause times scales. The fit distributions for various outlet sizes are shown in Fig. 3 of the main text.

B. Large outlet clogging time and effective noise scaling relation

As shown in Section S2, in the large outlet regime [where τ_F grows, see Fig. S1(c)], the average clogging time is $\langle T \rangle \approx \tau_F/p$. To compute τ_F from the Fokker-Planck equation, we note that the flow duration before a pause or clog does not depend significantly on $\epsilon \ll 1$, the noise added by the hidden mode $y = 1$. In other words, while the hidden variable state determines the stability of the clog, it has very little impact on the flow preceding the clog. Therefore, we can fix $y = 0$ and study the one-dimensional Fokker-Planck equation,

$$\frac{\partial P_0}{\partial t} = -\frac{\partial}{\partial x}(fP_0) + \frac{\partial^2}{\partial x^2}(gP_0).\tag{S15}$$

The mean time to hit a clog or pause state ($x = 0$) starting from initial flow rate x_i satisfies the adjoint equation [5],

$$f(x_i)\tau_F'(x_i) + g(x_i)\tau_F''(x_i) = -1,\tag{S16}$$

with an absorbing boundary at $x = 0$, $\tau_F(0) = 0$ and reflecting boundary at infinity, $\lim_{x \rightarrow \infty} \tau'_F(x) = 0$. The solution to this equation is

$$\tau_F(x_i) = \int_0^{x_i} dy \int_y^\infty dz \frac{e^{\Theta(y) - \Theta(z)}}{g(z)}, \quad (\text{S17})$$

where $\Theta(x) = -\int_0^x f(x')/g(x') dx'$. In our flow-rate distribution fits, the steady flow rate x_0 and noise amplitude grow proportionally so that the relative noise $\tilde{\Delta} = \Delta\tau_0/x_0^2$ shrinks for larger outlet sizes [see inset of Fig. 3(b) in the main text]. Thus when $D/d_L \gg 1$, we have $\tilde{\Delta} \ll 1$, which appears in the denominator of Θ . To approximate the flow duration in this regime, we can therefore evaluate the integrals in Eq. (S17) using a saddle-point approximation. For this analysis we consider deterministic force $f(x) = -x^2(x - x_0)\Psi(x)/(\tau_0 x_0^2)$ with an arbitrary deformation factor $\Psi(x)$. We require $\Psi(x) > 0$ and $\Psi(x_0) = 1$ so that the force has no additional roots and the linear correlation time near x_0 is always τ_0 .

The maximum of the exponent $\Theta(y) - \Theta(z)$ in Eq. (S17) within the integration domain occurs at $y_0 = 0$, $z_0 = x_0$. To quadratic order in $\delta y = y - y_0$, $\delta z = z - z_0$, the exponent becomes

$$\Theta(y) - \Theta(z) = -\Theta(x_0) - \frac{\Psi(0)}{2\Delta\tau_0}\delta y^2 - \frac{1}{2\Delta\tau_0}\delta z^2. \quad (\text{S18})$$

Thus, for $\tilde{\Delta} \ll 1$ the integral in Eq. (S17) reduces to a tightly peaked Gaussian integral around (y_0, z_0) . Evaluating the integral we find,

$$\langle T \rangle \sim \tau_F/p \sim \frac{2\pi\tau_0 p^{-1}}{\sqrt{\Psi(0)}} e^{-\Theta(x)} = \frac{2\pi\tau_0 p^{-1}}{\sqrt{\Psi(0)}} \exp\left(\frac{1}{\tilde{\Delta}} \int_0^1 \tilde{x}(1 - \tilde{x})\Psi(\tilde{x}x_0) d\tilde{x}\right), \quad (\text{S19})$$

where in the final expression, we have written the exponent explicitly in terms of the effective noise $\tilde{\Delta}$ and a constant integral. For example, with the force used to fit the experimental flow-rate distributions [Eq. (S14), with $\Psi(x) = (x^2 - 2ax + a^2 + b^2)/(x_0^2 - 2ax_0 + a^2 + b^2)$], we have

$$\langle T \rangle \sim 2\pi\tau_0 p^{-1} \sqrt{1 + \frac{1 - 2\tilde{a}}{\tilde{a}^2 + \tilde{b}^2}} \exp\left(\frac{1}{\tilde{\Delta}} \left[\frac{1}{6} + \frac{1}{60} \frac{10\tilde{a} - 7}{(\tilde{a} - 1)^2 + \tilde{b}^2}\right]\right), \quad (\text{S20})$$

where $\tilde{a} = a/x_0$ and $\tilde{b} = b/x_0$. Suppressing the constants, both Eqs. (S19) and (S20) have the form $\langle T \rangle \sim \tau_0 p^{-1} C \exp(c\tilde{\Delta}^{-1})$ quoted in the main text.

C. Clog prediction: first passage to zero flow rate and hidden variable dynamics

Finally, we can use the Fokker-Planck equation to explore whether it is possible to predict clogs given the current flow rate x and the state of the hidden variable y . To this end, we compute $p_0(x)$, the probability of flow rate hitting zero (either a pause or a clog) before returning to steady flow x_0 , starting from current flow rate x . We also compute the average time $t_0(x)$ to hit zero flow (conditioned on this occurring before the system resumes steady flow $x = x_0$), as a measure of how far in advance predictions can be made.

Just as in the preceding section, the flow trajectories before hitting the pause or clog ($x = 0$) or the steady flow state ($x = x_0$) are nearly independent of the hidden variable state y , since the ϵ addition to the noise is only relevant very close to 0. Therefore, we again focus on analyzing the one-dimensional system, Eq. (S15). The zero-flow hitting probability and time satisfy adjoint equations similar to Eq. (S16), but with two absorbing boundaries (i.e. the zero-flow $x = 0$ and steady flow $x = x_0$ states) [5],

$$f(x)p'_0(x) + g(x)p''_0(x) = 0 \quad f(x)\vartheta'_0(x) + g(x)\vartheta''_0(x) = -p_0(x). \quad (\text{S21})$$

Here $\vartheta_0(x) = p_0(x)t_0(x)$ and the boundary conditions are $p_0(0) = 1$, $p_0(x_0) = 0$, and $\vartheta_0(0) = \vartheta_0(x_0) = 0$. We numerically integrate these equations with force and noise parameters taken from the fits to the experimental flow-rate distributions at each outlet size.

Fig. S2(a) shows both the zero-flow hitting probability $p_0(x)$ and hitting time $t_0(x)$ for the full range of initial conditions $0 < x < x_0$. Accurate prediction of non-flowing events remains difficult due to the Markovian nature for the dynamics. For example, there is only a 75% chance to hit zero flow even when the flow rate is already quite slow

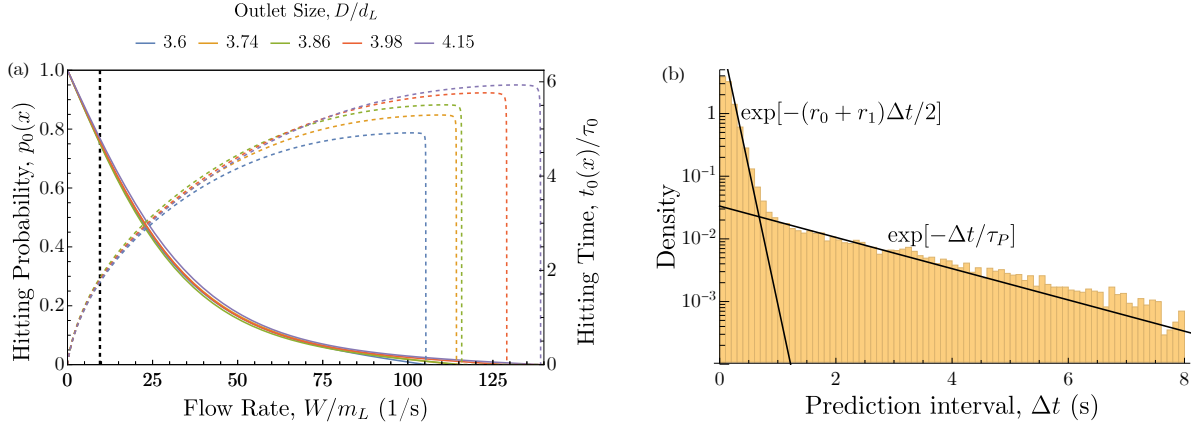


FIG. S2. *Predicting clogs.* (a) The probability $p_0(x)$ (solid curves) and average time $t_0(x)$ (dashed curves) for a granular flow with current rate $x = W/m_L$ to hit zero flow (clog or pause) before returning to steady flow rate x_0 . Curves computed by numerically solving Eq. (S21) with parameters fixed by fitting of the flow-rate distributions (main text, Fig. 3). The black dashed line shows the threshold for 75% probability at $x \approx 10 \text{ s}^{-1}$. (b) Distribution of times Δt since the last change in the hidden state y before a clog or pause. The distribution has two exponential time-scales $2/(r_0 + r_1)$ and τ_P , corresponding respectively to the average y switching rate and to cases where the flow un-pauses and quickly re-pauses without y changing state. The y -state enables distinguishing incipient clogs from pauses $\langle \Delta t \rangle = 0.27 \text{ s}$ ahead of time on average. Data from 10^5 simulated trajectories of the model fit to $D = 3.86d_L$ trajectories.

($x < 10 \text{ s}^{-1}$). Fig. S2(a) also shows the average time to hit zero flow is similar to the flow rate correlation time. When the prediction accuracy is 75%, the prediction time is less than $2\tau_0 \approx 40 \text{ ms}$.

Clog prediction is further confounded by the presence of pauses: even if the flow ceases, will it restart at a later time? In our model, the hidden variable freezes as the flow rate approaches zero, often well before a pause or clog [e.g. Fig.1(c) in the main text]. Fig. S2(b) shows the distribution of $\Delta t = t_{x=0} - t_{\delta y}$, the time interval between the onset of a pause or clog and the previous change in the state of y ; we find $\langle \Delta t \rangle = 0.27 \text{ s} \approx 12\tau_0$. If one could reliably predict zero-flow events, then monitoring the hidden variable state y would enable advanced determination of whether the incipient clog will be stable or unstable.

-
- [1] I. Zuriguel, D. R. Parisi, R. C. Hidalgo, C. Lozano, A. Janda, P. A. Gago, J. P. Peralta, L. M. Ferrer, L. A. Pugnali, E. Clément, D. Maza, I. Pagonabarraga, and A. Garcimartín, *Scientific reports* **4**, 7324 (2014).
 - [2] C. Merrigan, S. K. Birwa, S. Tewari, and B. Chakraborty, *Phys. Rev. E* **97**, 040901 (2018).
 - [3] R. Caitano, B. V. Guerrero, R. E. R. González, I. Zuriguel, and A. Garcimartín, *Phys. Rev. Lett.* **127**, 148002 (2021).
 - [4] B. V. Guerrero, B. Chakraborty, I. Zuriguel, and A. Garcimartín, *Phys. Rev. E* **100**, 032901 (2019).
 - [5] N. G. van Kampen, *Stochastic processes in physics and chemistry* (Elsevier, Amsterdam, 2007).